Report

Current Biology

Polarized Cell Motility Induces Hydrogen Peroxide to Inhibit Cofilin via Cysteine Oxidation

Highlights

- Cell migration leads to localized hydrogen peroxide generation
- Motility increases protein oxidation on cysteine residues
- Cofilin oxidation on Cys139 and Cys147 reduces actin binding and severing
- Oxidation of cofilin, and possibly additional proteins, influences cell motility

Authors

Jenifer M. Cameron, Mads Gabrielsen, ..., Huabing Yin, Michael F. Olson

Correspondence

m.olson@beatson.gla.ac.uk

In Brief

Cell migration is regulated by signaling events that regulate protein activity. Here, Cameron et al. imaged highest H_2O_2 levels in motile cell protrusions, accompanied by cysteine oxidation of proteins, including actin-regulating cofilin. Cofilin oxidation reduced actin binding and severing, linking H_2O_2-generation with cytoskeleton dynamics.

Cameron et al., 2015, Current Biology *25*, 1520–1525
June 1, 2015
http://dx.doi.org/10.1016/j.cub.2015.04.020

CellPress

CellPress

Current Biology
Report

Polarized Cell Motility Induces Hydrogen Peroxide to Inhibit Cofilin via Cysteine Oxidation

Jenifer M. Cameron,[1] Mads Gabrielsen,[1] Ya Hua Chim,[2] June Munro,[1] Ewan J. McGhee,[1] David Sumpton,[1] Philip Eaton,[3] Kurt I. Anderson,[1] Huabing Yin,[2] and Michael F. Olson[1,*]

[1]Cancer Research UK Beatson Institute, Garscube Estate, Switchback Road, Glasgow G61 1BD, UK
[2]Division of Biomedical Engineering, School of Engineering, University of Glasgow, Glasgow G12 8LT, UK
[3]Cardiovascular Division, The Rayne Institute, St. Thomas' Hospital, King's College London, London SE1 7EH, UK
*Correspondence: m.olson@beatson.gla.ac.uk
http://dx.doi.org/10.1016/j.cub.2015.04.020

SUMMARY

Mesenchymal cell motility is driven by polarized actin polymerization [1]. Signals at the leading edge recruit actin polymerization machinery to promote membrane protrusion, while matrix adhesion generates tractive force to propel forward movement. To work effectively, cell motility is regulated by a complex network of signaling events that affect protein activity and localization. H_2O_2 has an important role as a diffusible second messenger [2], and mediates its effects through oxidation of cysteine thiols. One cell activity influenced by H_2O_2 is motility [3]. However, a lack of sensitive and H_2O_2-specific probes for measurements in live cells has not allowed for direct observation of H_2O_2 accumulation in migrating cells or protrusions. In addition, the identities of proteins oxidized by H_2O_2 that contribute to actin dynamics and cell motility have not been characterized. We now show, as determined by fluorescence lifetime imaging microscopy, that motile cells generate H_2O_2 at membranes and cell protrusions and that H_2O_2 inhibits cofilin activity through oxidation of cysteines 139 (C139) and 147 (C147). Molecular modeling suggests that C139 oxidation would sterically hinder actin association, while the increased negative charge of oxidized C147 would lead to electrostatic repulsion of the opposite negatively charged surface. Expression of oxidation-resistant cofilin impairs cell spreading, adhesion, and directional migration. These findings indicate that H_2O_2 production contributes to polarized cell motility through localized cofilin inhibition and that there are additional proteins oxidized during cell migration that might have similar roles.

RESULTS AND DISCUSSION

H_2O_2 Is Elevated in Migrating Cell Protrusions

To determine whether H_2O_2 is increased in motile cells, we imaged cytoplasmic and plasma-membrane-targeted forms of the HyPer probe (HyPer-cyto and HyPer-PM; Figures S1A–S1G and S2A–S2E) [4, 5] by fluorescence lifetime imaging microscopy (FLIM) [6]. Confluent monolayers were wounded and HyPer fluorescence lifetimes were measured in migrating and stationary cells. HyPer-cyto and HyPer-PM fluorescence lifetimes were significantly reduced in migrating cells, indicating higher cytoplasmic and plasma membrane H_2O_2 (Figures 1A and 1B). H_2O_2 was also higher in protrusions, relative to cell bodies, of migrating HyPer-cyto-expressing cells (Figures 1C and 1D), indicating that H_2O_2 is elevated in migrating cells, with highest levels in protrusions.

Protein Oxidation in Cell Migration

Cell-permeable 5,5-dimethyl-1,3-cyclohexanedione (dimedone) was used to label oxidized proteins by irreversible reaction with cysteine sulfenic acid (Figure 2A) [7, 8]. Stationary confluent cells and scratch-wounded migrating cells were left for 3 hr and then incubated with or without 5 mM dimedone for 1 hr (Figure 2B). Increased dimedone incorporation indicated that cell migration promotes protein oxidation.

For identification of oxidized proteins, a filter-aided sample preparation (FASP) method [9] concentrated proteins prior to tryptic digestion, followed by tandem mass spectrometry (MS). Dimedone-conjugated peptides were identified by searching for 138-Da mass-to-charge shifts rather than post-lysis 57-Da iodoacetamide-induced shifts. Actin-regulating cofilin was identified with dimedone labeling on cysteines 139 (C139) (Figure 2C) and 147 (C147) (data not shown). Immunoprecipitation and western blotting revealed that cofilin was more dimedone labeled in migrating relative to stationary cells (Figures 2D and 2E).

C139 and C147 Oxidation Inhibits Cofilin Activity

Cofilin regulates cytoskeletal dynamics through activities including G-actin sequestration [10]. Based on the human cofilin structure (PDB: 4BEX) [11] and G-actin associated with the twinfilin C-terminal cofilin-like domain (PDB: 3DAW) [12], a cofilin/G-actin model predicts C139 and C147 at the binding interface (Figure 3A). Oxidation increases their van der Waals radii (Figure 3B), which could block actin binding, particularly for C139 that sits adjacent to actin K328 (Figure 3A). Electrostatic surface potential mapping suggests that C139 and C147 (Figure S3A) oxidation to sulfenic (Figure S3IB) or sulfinic acid (Figure S3C) would increase negative charges such that consequent

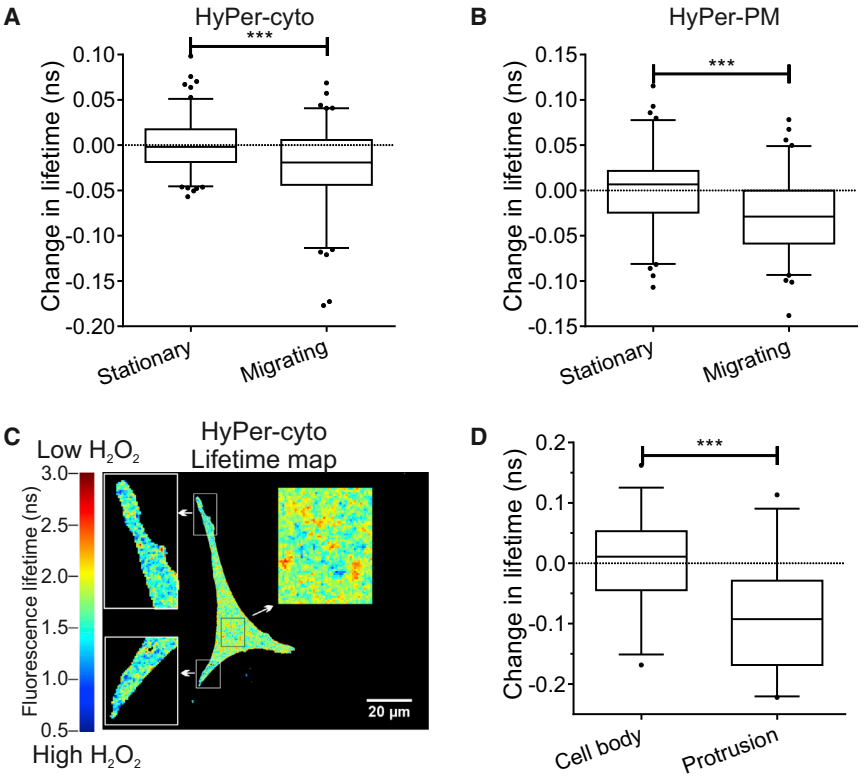

Figure 1. Elevated H_2O_2 in Motile Cell Protrusions

(A) HyPer-cyto fluorescence lifetime changes (t test, ***$p < 0.001$). Upper and lower quartiles define box with median line, 5%–95% range whiskers. n = 102 stationary and 130 migrating cells. See also Figure S1.

(B) HyPer-PM fluorescence lifetime changes (t test, ***$p < 0.001$). Upper and lower quartiles define box with median line, 5%–95% range whiskers. n = 83 stationary and 83 migrating cells. See also Figures S1 and S2.

(C) MDAMB231 cell expressing HyPer-cyto showing fluorescence lifetime heatmap throughout cell body and protrusions. Higher magnification insets of the indicated regions.

(D) HyPer-cyto fluorescence lifetime changes (t test, ***$p < 0.001$). Upper and lower quartiles define box with median line, 5%–95% range whiskers. n = 29 cell bodies and 36 protrusions of migrating cells.

electrostatic repulsion with actin surface residues, such as E241 located adjacent to cofilin C147, could impair binding. Recombinant cofilin bound G-actin-ATP at a 1:1 ratio with 2.0 μM binding affinity ($1/K_A$) by isothermal titration calorimetry (ITC; Figure 3C), approaching previous values [13]. C139 and C147 were mutated to aspartic acid (C139D/C147D), with their β-carboxylic acid mimicking the increased side-chain volume and negative charge of sulfinic acid. C139D/C147D protein folding was validated by thermal shift assay (Figure S3D) [14], but G-actin binding was not detected by ITC (Figure 3D), indicating decreased affinity.

Pelleting equivalent F-actin (21 μM) by ultracentrifugation revealed that associated WT cofilin was significantly reduced by 10 mM H_2O_2 pre-treatment (Figures 3E and 3F). However, C139A/C147A (AA) cofilin resisted the H_2O_2-induced reduction in F-actin association (Figures 3E and 3F). Pelleting 10 μM F-actin with varying cofilin concentrations, with or without 10 mM H_2O_2 pre-treatment, revealed ~7-fold lower associated cofilin after oxidation (Figure 3G). These results indicate that oxidation inhibits cofilin binding to F-actin, consistent with reduced actin-cofilin binding following taurine chloramine treatment of lymphoma cells to induce cofilin oxidation [15].

For analysis of how cofilin oxidation affected F-actin regulation, ultracentrifugation separated 21 μM actin into G-actin supernatant (S) and F-actin pellet (P) fractions [16]. G-actin was entirely in the S fraction, while polymerization redistributed F-actin toward the P fraction (Figure 3H). Addition of 10 μM cofilin shifted F-actin toward the G-actin S fraction, which was inhibited by 10 mM H_2O_2 pre-treatment (Figure 3H). Next, immobilized rhodamine-labeled 2 μM F-actin was incubated for 30 min with no addition (Figure 3I, left), 1 μM cofilin (Figure 3I, middle), or H_2O_2 pre-treated cofilin (Figure 3I, right). Determination of occurrence of F-actin filament lengths is described in Supplemental Information. Untreated cofilin reduced the number of long F-actin filaments (>0.5 μm), while 10 mM H_2O_2 pre-treatment partially inhibited this effect on filaments >2.5 μm and completely blocked the reduction in filaments between 0.5 and 2.5 μm (Figure 3J). These results indicate that cofilin oxidation reduced F-actin severing. Further support for this conclusion is based on pyrene-actin assays described in Figures S3E–S3K. Interestingly, C139 and C147 are not conserved in cofilin2 or actin-depolymerizing factor (ADF), or in cofilin homologs across kingdoms, suggesting that regulation by oxidation may be restricted to cofilin and only in higher species [11, 17]

Cofilin Oxidation Contributes to Adhesion and Directional Cell Migration

Dynamic and spatially restricted cofilin regulation of F-actin is required for membrane protrusions that promote cell spreading and adhesion [18, 19]. The role of cofilin inactivation by oxidation in cells was determined by comparing the effects of wild-type or oxidation-resistant cofilin expression. The cell index (CI) parameter, which reflects spreading and adhesion [20], was measured for MDAMB231 cells expressing mCherry fluorescent protein (Cherry), mCherry-cofilin (Ch-CFL), or oxidation-resistant mCherry-cofilin C139/147A [Ch-CFL(AA)] (Figure S4A). During the 3 hr after plating, Ch-CFL(AA) cells had significantly lower CI than Cherry or Ch-CFL cells (Figures 4A and 4B), indicating reduced adhesion, spreading, or both. To determine whether C139 or C147 oxidation was sufficient for this effect, we compared mCherry-cofilin C139A [Ch-CFL(C139A)] or mCherry-cofilin C147A [Ch-CFL(C147A)] (Figure S4B) CI measurements with those of wild-type Ch-CFL. Although each substitution trended toward decreased CI, neither was statistically significant (Figures 4C and 4D). Ch-CFL(AA) cells had significantly reduced adhesion 3 hr after plating (Figure 4E) that paralleled decreased

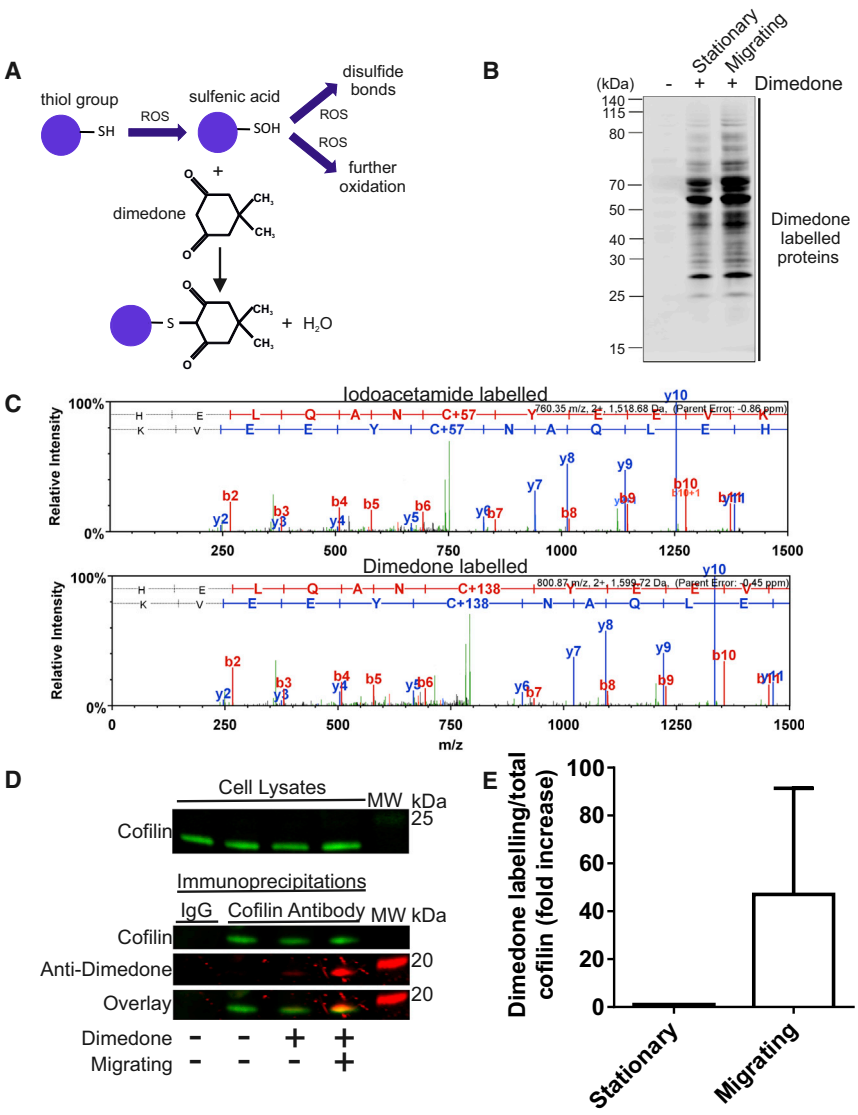

Figure 2. Cell Migration Leads to Protein Oxidation

(A) Schematic diagram of dimedone reaction with cysteine sulfenic acid.

(B) Western blot with dimedone-sulfenic acid antibody of MDAMB231 stationary or migrating cell lysates with or without dimedone incubation. Migration was induced by scratching with a P10 pipette tip, and then 3 hr was allowed prior to 1 hr of dimedone labeling. See also Figure S2.

(C) Fragmentation spectra from tandem MS of cofilin peptide 133–144 following in vitro iodoacetamide labeling (upper panel) or dimedone labeling in cells (lower panel). C139 was shifted by 57 Da by iodoacetamide or 138 Da by dimedone.

(D) Immunoprecipitation with control immunoglobin G (IgG) or anti-cofilin antibody followed by western blotting with dimedone-sulfenic acid and cofilin antibodies revealed increased dimedone labeling in migrating relative to stationary cells.

(E) Fold increase of dimedone-labeled cofilin over total cofilin for migrating cells relative to stationary cells (mean ± SEM, n = 3).

CI (Figure 4B), suggesting that reduced adhesion contributed to lower CI. Actin dynamics also contribute to cell stiffness [21, 22]. Nanoindentation with atomic force microscopy (AFM) [23] revealed that Ch-CFL or Ch-CFL(AA) expression both significantly increased the Young's elastic modulus of individual MDAMB231 cells (Figure 4F), indicating that cofilin functions independent of C139/C147 oxidation to regulate cell stiffness. Tracking two-dimensional (2D) individual cell movement for 4 hr after plating revealed that overall speeds of Cherry (Figure 4G), Ch-CFL (Figure 4H), and Ch-CFL(AA) (Figure 4I) cells were unaffected, but directional motility of Ch-CFL(AA)-expressing cells was significantly reduced relative to Cherry-expressing cells (Figure 4J), indicating that localized cofilin oxidation contributes to maintaining persistent cell movement.

We propose that H_2O_2 is generated at migrating cell leading edges, and consequently oxidation of proteins such as cofilin is increased. Oxidation on C139/C147 reduces cofilin activity, thereby enhancing either or both F-actin stability and net actin polymerization proximal to the front. Consistent with this, instantaneous chromophore-assisted laser inactivation revealed that active cofilin normally promotes lamellipodial F-actin turnover [24]. An additional potential contributing factor is that oxidized cofilin at plasma membranes is likely to be inactivated by membrane lipid association, unlike reduced cofilin that was shown to be insensitive to phosphatidylinositol 4,5-bisphosphate (PIP_2)-induced inhibition [25]. Furthermore, cofilin oxidation might reduce competition with myosin II for F-actin binding, thereby enabling development of actin-myosin cortical tension that contributes to cell motility independent of F-actin turnover [26]. Localized control of cofilin activity through oxidation enables cells to harness actin-myosin dynamics required for directional migration. Consistent with this, externally applied H_2O_2 increased F-actin retrograde flow, cell protrusions, and directional migration [27]. The number of proteins oxidized during cell migration (Figure 2E) suggests that more proteins regulated in this manner may contribute to actin cytoskeletal dynamics.

SUPPLEMENTAL INFORMATION

Supplemental Information includes Supplemental Experimental Procedures and four figures and can be found with this article online at http://dx.doi.org/10.1016/j.cub.2015.04.020.

ACKNOWLEDGMENTS

This research was supported by Cancer Research UK and the Engineering and Physical Sciences Research Council. We thank L. Machesky and H. Spence for purified actin and A.W. Schüttelkopf for assistance with the charge calculations.

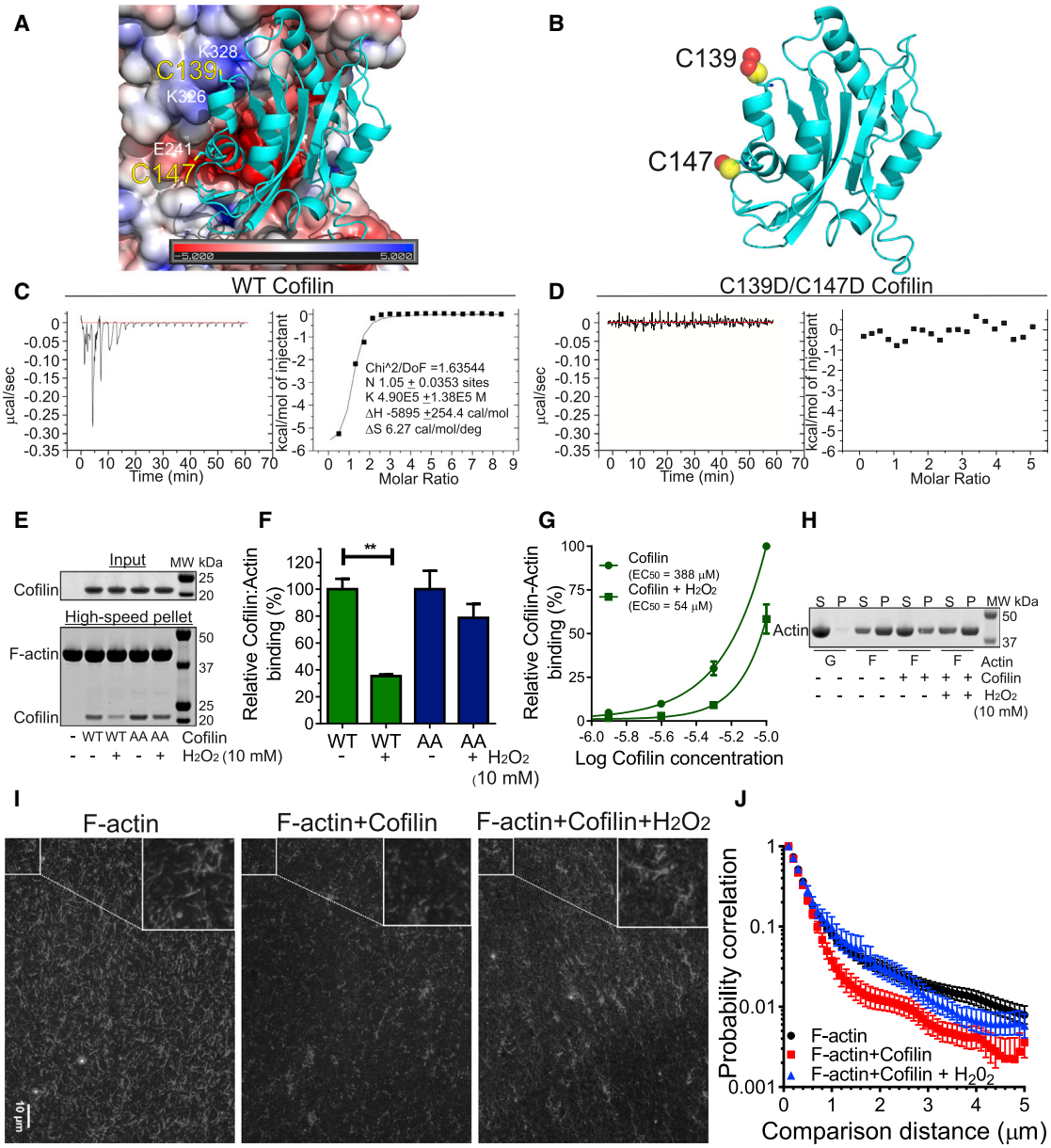

Figure 3. Oxidation on C139 and C147 Reduces Cofilin Activity

(A) Modeling of human cofilin (ribbon) and actin (space-filled electrostatic potential map, color coding shows range away from neutral in kT/e) interaction. C139 (yellow; upper stick with yellow sulfur) is near actin K328 (white), while C147 (yellow) is near negatively charged E241 (white). See also Figure S3.

(B) C139 and C147 oxidation (red spheres) to sulfinic acid increases van der Waals radii and potential steric interference with actin binding.

(C) ITC measurement of binding stoichiometry (N), binding affinity (K), enthalpy change (ΔH), and entropy change (ΔS) for wild-type (WT) cofilin binding to G-actin (30 µM). Left: heat released after 2-µl injections of 1.2 mM cofilin over time. Right: binding curve fitted for ratios of cofilin and actin used. Chi-square per degrees of freedom (Chi^2/DoF) indicates goodness of fitted curve.

(D) ITC determination for C139D/C147D cofilin as in (C).

(E) Ultracentrifugation pelleting of 21 µM F-actin with 10 µM WT or C139/147A (AA) cofilin co-sedimentation, with or without H_2O_2 treatment.

(F) Relative cofilin binding (mean ± SEM, n = 3) of 10 µM WT (green; t test, **$p < 0.01$) or C139/147A (AA) protein (blue), with or without H_2O_2 treatment, to 21 µM F-actin.

(G) Amount of untreated (circles) or 10 mM H_2O_2-treated (squares) cofilin (mean ± SEM, n = 3) pelleted with 1 µM F-actin by ultracentrifugation relative to amount pelleted from 10 µM untreated cofilin.

(H) Total of 21 µM G-actin (G) or F-actin (F) separated into S or P fractions by ultracentrifugation. Cofilin (10 µM) shifted F-actin toward the S fraction, which was reduced by 10 mM H_2O_2.

(I) Immobilized rhodamine-labeled F-actin (2 µm) incubated for 30 min with buffer (left), 1 µm cofilin (middle), or 1 µm cofilin pre-treated with 10 mM H_2O_2 (right). Insets in top left corners are magnified in top right corners. The scale bar represents 10 µm

(J) Actin filament length determined from replicate images by gray-level co-occurrence matrix (GLCM) correlations. Probability correlations (mean ± SEM, n = 9–14) versus co-occurrence distance are shown for 2 µM F-actin incubated alone (black circles), with 1 µM untreated cofilin (red squares), or with 1 µm cofilin pre-treated with 10 mM H_2O_2 (blue triangles).

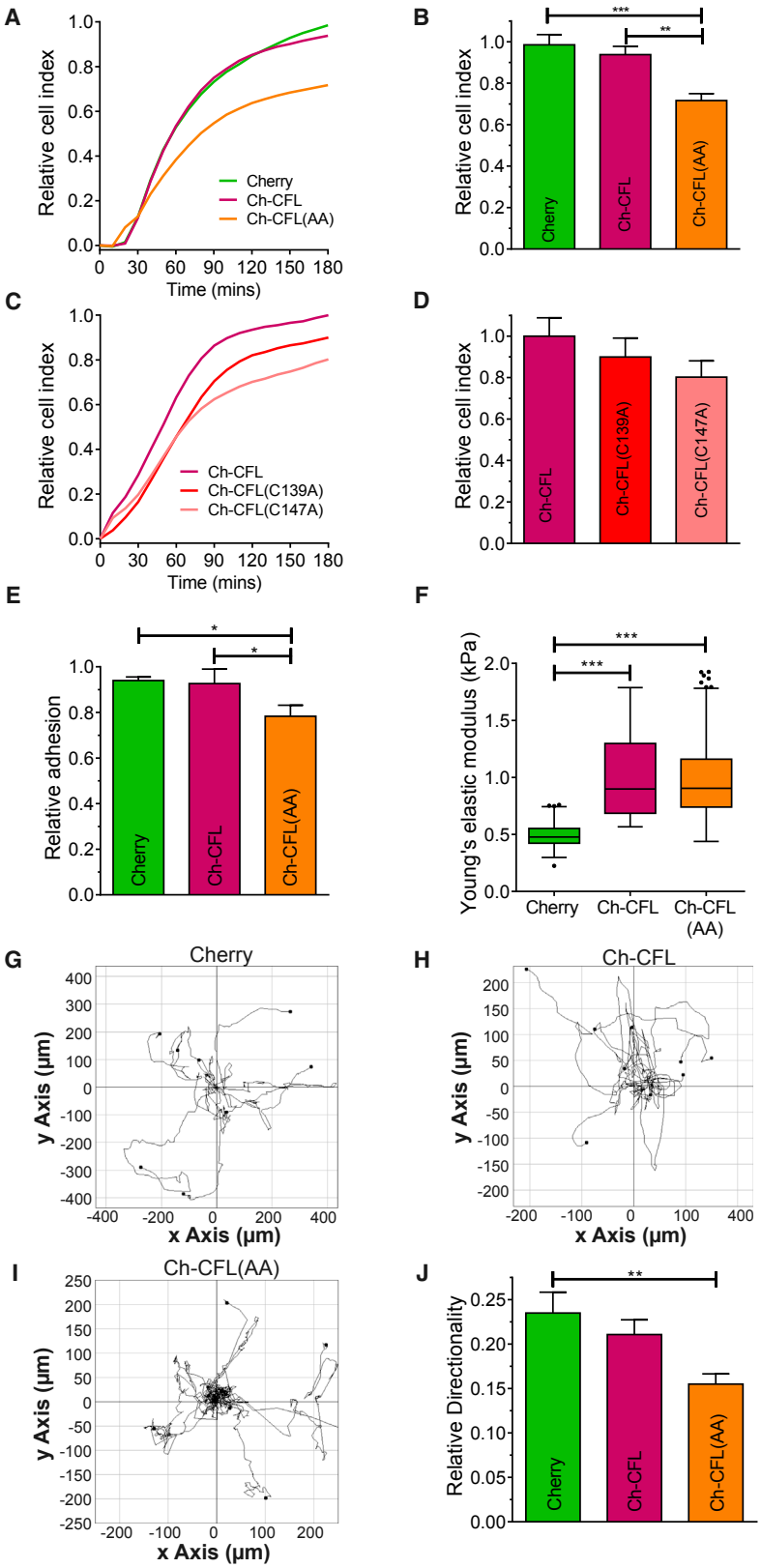

Figure 4. Oxidation-Resistant Cofilin Reduces Cell Adhesion and Directional Motility

(A) Kinetic cell index determinations for Cherry-, Ch-CFL-, or Ch-CFL(AA)-expressing cells over 3 hr. See also Figure S4.

(B) Cell index values (mean ± SEM, n = 5). One-way ANOVA followed by Tukey's post hoc test (***p < 0.001, **p < 0.01) at 3-hr endpoint relative to parental cells (set to 1 for each determination) reflects either or both decreased cell spreading and adhesion for Ch-CFL(AA).

(C) Kinetic cell index determinations for Ch-CFL-, Ch-CFL(C139A)-, or Ch-CFL(C147A)-expressing cells over 3 hr. See also Figure S4.

(D) Cell index values (mean ± SEM, n = 4) at 3-hr endpoint relative to Ch-CFL cells (set to 1 for each determination).

(E) Relative adhesion (mean ± SEM, n = 3). One-way ANOVA followed by Tukey's post hoc test (*p < 0.05) of Cherry-, Ch-CFL-, or Ch-CFL(AA)-expressing cells was determined by staining vigorously washed cells 3 hr after plating.

(F) Elasticity measurements by nanoindentation with atomic force microscopy for >340 cells per condition. One-way ANOVA followed by Tukey's post hoc test (***p < 0.001). Upper and lower quartiles define box with median line, Tukey range whiskers.

(G–I) Spider plots of random migration over 4 hr for cells expressing Cherry (G), Ch-CFL (H), or Ch-CFL(AA) (I).

(J) Random cell migration directionality determined for 12 independent fields with 10–20 migrating cells per field. Directionality is ratio of Euclidean over accumulated distance traveled. Data shown indicate mean ± SEM. One-way ANOVA followed by Tukey's post hoc test (**p < 0.01).

Received: January 30, 2014
Revised: March 10, 2015
Accepted: April 13, 2015
Published: May 14, 2015

REFERENCES

1. Olson, M.F., and Sahai, E. (2009). The actin cytoskeleton in cancer cell motility. Clin. Exp. Metastasis *26*, 273–287.
2. Forman, H.J., Maiorino, M., and Ursini, F. (2010). Signaling functions of reactive oxygen species. Biochemistry *49*, 835–842.
3. Hurd, T.R., DeGennaro, M., and Lehmann, R. (2012). Redox regulation of cell migration and adhesion. Trends Cell Biol. *22*, 107–115.
4. Belousov, V.V., Fradkov, A.F., Lukyanov, K.A., Staroverov, D.B., Shakhbazov, K.S., Terskikh, A.V., and Lukyanov, S. (2006). Genetically encoded fluorescent indicator for intracellular hydrogen peroxide. Nat. Methods *3*, 281–286.
5. Wright, L.P., and Philips, M.R. (2006). Thematic review series: lipid post-translational modifications. CAAX modification and membrane targeting of Ras. J. Lipid Res. *47*, 883–891.
6. Weller, J., Kizina, K.M., Can, K., Bao, G., and Müller, M. (2014). Response properties of the genetically encoded optical H2O2 sensor HyPer. Free Radic. Biol. Med. *76*, 227–241.
7. Allison, W.S. (1976). Formation and reactions of sulfenic acids in proteins. Acc. Chem. Res. *9*, 293–299.
8. Maller, C., Schröder, E., and Eaton, P. (2011). Glyceraldehyde 3-phosphate dehydrogenase is unlikely to mediate hydrogen peroxide signaling: studies with a novel anti-dimedone sulfenic acid antibody. Antioxid. Redox Signal. *14*, 49–60.
9. Wiśniewski, J.R., Zougman, A., Nagaraj, N., and Mann, M. (2009). Universal sample preparation method for proteome analysis. Nat. Methods *6*, 359–362.
10. Bravo-Cordero, J.J., Magalhaes, M.A.O., Eddy, R.J., Hodgson, L., and Condeelis, J. (2013). Functions of cofilin in cell locomotion and invasion. Nat. Rev. Mol. Cell Biol. *14*, 405–415.
11. Klejnot, M., Gabrielsen, M., Cameron, J., Mleczak, A., Talapatra, S.K., Kozielski, F., Pannifer, A., and Olson, M.F. (2013). Analysis of the human cofilin 1 structure reveals conformational changes required for actin binding. Acta Crystallogr. D Biol. Crystallogr. *69*, 1780–1788.
12. Paavilainen, V.O., Oksanen, E., Goldman, A., and Lappalainen, P. (2008). Structure of the actin-depolymerizing factor homology domain in complex with actin. J. Cell Biol. *182*, 51–59.
13. De La Cruz, E.M., and Sept, D. (2010). The kinetics of cooperative cofilin binding reveals two states of the cofilin-actin filament. Biophys. J. *98*, 1893–1901.
14. Lavinder, J.J., Hari, S.B., Sullivan, B.J., and Magliery, T.J. (2009). High-throughput thermal scanning: a general, rapid dye-binding thermal shift screen for protein engineering. J. Am. Chem. Soc. *131*, 3794–3795.
15. Klamt, F., Zdanov, S., Levine, R.L., Pariser, A., Zhang, Y., Zhang, B., Yu, L.R., Veenstra, T.D., and Shacter, E. (2009). Oxidant-induced apoptosis is mediated by oxidation of the actin-regulatory protein cofilin. Nat. Cell Biol. *11*, 1241–1246.
16. Gabrielsen, M., Schuldt, M., Munro, J., Borucka, D., Cameron, J., Baugh, M., Mleczak, A., Lilla, S., Morrice, N., and Olson, M.F. (2013). Cucurbitacin covalent bonding to cysteine thiols: the filamentous-actin severing protein Cofilin1 as an exemplary target. Cell Commun. Signal. *11*, 58.
17. Vartiainen, M.K., Mustonen, T., Mattila, P.K., Ojala, P.J., Thesleff, I., Partanen, J., and Lappalainen, P. (2002). The three mouse actin-depolymerizing factor/cofilins evolved to fulfill cell-type-specific requirements for actin dynamics. Mol. Biol. Cell *13*, 183–194.
18. Parsons, J.T., Horwitz, A.R., and Schwartz, M.A. (2010). Cell adhesion: integrating cytoskeletal dynamics and cellular tension. Nat. Rev. Mol. Cell Biol. *11*, 633–643.
19. Ridley, A.J. (2011). Life at the leading edge. Cell *145*, 1012–1022.
20. Rahim, S., and Üren, A. (2011). A real-time electrical impedance based technique to measure invasion of endothelial cell monolayer by cancer cells. J. Vis. Exp. *50*, 2792.
21. Tsai, M.A., Waugh, R.E., and Keng, P.C. (1998). Passive mechanical behavior of human neutrophils: effects of colchicine and paclitaxel. Biophys. J. *74*, 3282–3291.
22. Salbreux, G., Charras, G., and Paluch, E. (2012). Actin cortex mechanics and cellular morphogenesis. Trends Cell Biol. *22*, 536–545.
23. McPhee, G., Dalby, M.J., Riehle, M., and Yin, H. (2010). Can common adhesion molecules and microtopography affect cellular elasticity? A combined atomic force microscopy and optical study. Med. Biol. Eng. Comput. *48*, 1043–1053.
24. Vitriol, E.A., Wise, A.L., Berginski, M.E., Bamburg, J.R., and Zheng, J.Q. (2013). Instantaneous inactivation of cofilin reveals its function of F-actin disassembly in lamellipodia. Mol. Biol. Cell *24*, 2238–2247.
25. Schulte, B., John, I., Simon, B., Brockmann, C., Oelmeier, S.A., Jahraus, B., Kirchgessner, H., Riplinger, S., Carlomagno, T., Wabnitz, G.H., and Samstag, Y. (2013). A reducing milieu renders cofilin insensitive to phosphatidylinositol 4,5-bisphosphate (PIP2) inhibition. J. Biol. Chem. *288*, 29430–29439.
26. Wiggan, O., Shaw, A.E., DeLuca, J.G., and Bamburg, J.R. (2012). ADF/cofilin regulates actomyosin assembly through competitive inhibition of myosin II binding to F-actin. Dev. Cell *22*, 530–543.
27. Taulet, N., Delorme-Walker, V.D., and DerMardirossian, C. (2012). Reactive oxygen species regulate protrusion efficiency by controlling actin dynamics. PLoS ONE *7*, e41342.